ACS OMEGA

Article

Cite This: ACS Omega 2017, 2, 9288−9295

Thenoyltrifluoroacetone (TTA)−Carbon Dot/Aerogel Fluorescent Sensor for Lanthanide and Actinide Ions

Susmita Dolai,[†] Susanta Kumar Bhunia,[†,∥] Leila Zeiri,[‡] Ofra Paz-Tal,[*,§] and Raz Jelinek[*,†,‡]

[†]Department of Chemistry and [‡]Ilse Katz Institute for Nanotechnology, Ben Gurion University of the Negev, Beer Sheva 84105, Israel

[§]Chemistry Department, Nuclear Research Center, Negev, P.O. Box 9001, Beer Sheva 84190, Israel

Supporting Information

ABSTRACT: Contamination of groundwater with radioactive substances comprising actinides and lanthanides is a significant environmental hazard and thus the development of selective, sensitive, and easy-to-apply sensors for water-soluble actinide and lanthanide ions is highly sought. We constructed a new selective fluorescent sensor for UO_2^{2+}, Sm^{3+}, and Eu^{3+} based on a carbon dot (C-dot)−aerogel hybrid prepared through in situ carbonization of 2-thenoyltrifluoroacetone (TTA), a high-affinity heavy metal chelator. The TTA−C-dot−aerogel enabled the detection of UO_2^{2+} ions, which induced a significant red fluorescence shift, whereas Eu^{3+} and particularly Sm^{3+} ions gave rise to pronounced fluorescence quenching. Importantly, the lanthanide/actinide ion-selective TTA−C-dots could be synthesized only in situ inside the aerogel pores, indicating the crucial role of the aerogel host matrix both in enabling the formation of the C-dots and in promoting the adsorption and interactions of the lanthanide and actinide metal ions with the embedded C-dots.

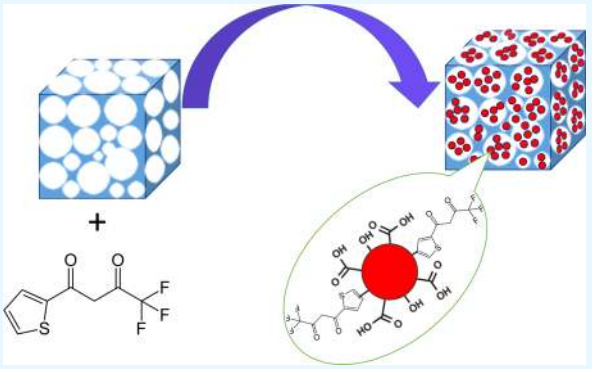

INTRODUCTION

Varied industries and utilities such as coal and phosphate mines, fossil fuel power plants, and others generate substantial amounts of natural albeit hazardous toxic metal ions in soil and groundwater.[1] Environmental contamination with radioactive species such as actinide ion UO_2^{2+} and long half-life lanthanide fission products such as $^{151}Sm^{3+}$ might also occur through intentional or accidental leakage (e.g., the nuclear accidents in Chernobyl and Fukushima). Human exposure to these ions occurs through the oral, dermal, wound, or respiratory routes, significantly increasing the risks of health hazards, including carcinogenesis, tissue fibrosis, and pneumoconiosis.[2−4] Accordingly, the development of sensors that can report on the presence of lanthanide and actinide ions is critical for alerting and implementation of strategies for the remediation of contaminated materials.[5,6]

Varied methods have been developed for the detection of lanthanides and actinides, including potentiometric membrane sensors,[7] sensing platforms based on colorimetric gold nanoparticles,[8] fluorescent molecular dyes,[9,10] conjugated polymer sensors,[11] and so on. Fluorescent sensors, in particular, exhibit practical advantages for metal ion detection in terms of sensitivity, selectivity, easy operation, low cost, and availability of multiple sensing parameters.[5,12] However, although numerous fluorescent sensors for metal ions have been reported over the past several years,[13−15] sensitive and selective fluorescence sensors for the detection of lanthanide and actinide metal ions are scarce. Specifically, significant practical limitations of lanthanide and actinide sensors have been encountered, including elaborate synthesis schemes, high cost of devices, and insufficient selectivity and/or sensitivity.[12,16]

Carbon dots (C-dots) constitute a family of fluorescent carbonaceous nanoparticles (<10 nm) and have attracted significant interest because of their unique structural and photophysical properties.[17−19] C-dots can be synthesized from inexpensive and readily available reagents using simple carbonization procedures.[20−22] Importantly, C-dots exhibit a broad range of excitation-dependent emission spectra, which are sensitive to the local environments of the dots, making possible the diverse sensing applications. In particular, metal ion sensing with C-dots has been reported.[23−25] An important aspect of C-dot chemistry in the context of sensing applications is the observation that these nanoparticles retain "structural memory" of the carbonaceous precursors, effectively endowing the dots with molecular recognition capabilities on the basis of functional units of the precursor molecules.[21] This remarkable feature has been employed for designing varied C-dot-based sensing modalities.[21,26,27]

Received: November 29, 2017
Accepted: December 15, 2017
Published: December 29, 2017

DOI: 10.1021/acsomega.7b01883
ACS Omega 2017, 2, 9288−9295

Here, we report the construction of a new lanthanide and actinide ion sensor comprising silica aerogel embedding C-dots prepared from 2-thenoyltrifluoroacetone (abbreviated TTA) as the carbonaceous building block. TTA, a β-diketone ligand (Scheme 1), has been employed as a scavenger for varied metal

Scheme 1. Structure of the 2-Thenoyltrifluoroacetone (TTA) Ligand

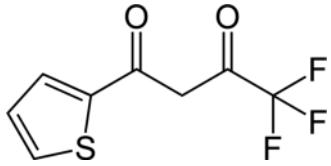

ions through chelating, forming relatively stable, insoluble complexes in aqueous solutions and organic solvents.[28,29] TTA has been employed as a chelator for lanthanide and actinide ions.[30] In particular, the ligand facilitated extraction of the ions in highly acidic solutions.[31] TTA has been also used as a conduit for sensing applications; low uranium concentrations could be detected, for example, via the luminescence properties of uranyl–TTA complexes.[32]

Importantly, the TTA-based C-dots were synthesized directly within the pores of an aerogel framework. Aerogels, among the lowest density solids known, constitute excellent materials for sensing applications because of their porous structures and very high internal surface area available for the adsorption of guest molecules.[33,34] Varied types of aerogels have been synthesized, comprising silicon, carbon, metal ions, organic polymers, and so on.[34−38] Hydrophobic silica aerogels, in particular, have been used as insulation materials in the aerospace industry,[39] in the sorption of miscible organic solvents in water,[40] and as sensors for varied analytes both in solution and in the gas phase.[41,42]

The new hybrid aerogel, encapsulating in situ TTA-generated C-dots, is capable of reporting on specific lanthanide and actinide ions in water. We show that the fluorescence of the aerogel-embedded solid-phase TTA–C-dots underwent ion-specific quenching or distinct red shifts. The TTA–C-dot–aerogel construct is resilient, easy to produce in large quantities, and could be effectively used as a platform for the detection and speciation of lanthanide and actinide metal ions.

RESULTS AND DISCUSSION

Synthesis and Characterization of the TTA–C-Dot–Aerogel. Figure 1 illustrates the simple in situ TTA–C-dot–aerogel fabrication method. The aerogel host matrix was prepared through high-temperature silica annealing in the presence of pressurized nitrogen gas.[42] After aerogel synthesis and drying, the TTA precursor was infiltrated into the aerogel pores through incubation in a diethyl ether–water mixture and heating to generate the aerogel-embedded C-dots. The TTA–C-dot–aerogel consisted of easy-to-handle coarse powder, and it was resilient and stable at room temperature for long time periods (months).

Figure 2 presents the spectroscopic and analytical characterizations of the TTA–C-dot/aerogel hybrid, both confirming the formation of C-dots within the aerogel pores and retaining the porous aerogel framework. Typical excitation-dependent emission spectra were recorded for C-dots inside the aerogel host (Figure 2A). Notably, significantly lower fluorescence

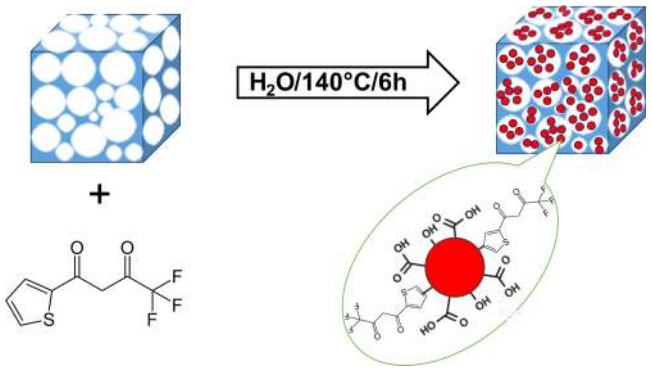

Figure 1. Synthesis of the TTA–carbon-dot–aerogel. The TTA precursor was initially incubated with the aerogel matrix. Subsequent carbonization resulted in the formation of carbon dots inside the aerogel pores. The red dots represent the graphitic carbon cores of the C-dots, whereas residual TTA was retained on the surface of C-dots.

emission, exhibiting different shifts, was acquired when the C-dots were hydrothermally synthesized from TTA in aqueous solution in the absence of aerogel (Figure S1). This observation indicates significant aggregation of TTA–C-dots in solution and concomitant quenching of C-dots fluorescence, attesting to the crucial role of the aerogel matrix in C-dot formation and stabilization.

The high-resolution transmission electron microscopy (HRTEM) images of the TTA–C-dots extracted from the aerogel matrix underscore the nanoscale dimensionality and crystalline nature of the carbon nanoparticles (Figure 2B). The HRTEM image shown in Figure 2B reveals a relatively uniform size distribution of the TTA–C-dots; C-dot diameters of 2.1 ± 0.5 nm were determined through the examination of several TEM images (Figure S2). The HRTEM image shown in Figure 2B (right) underscores the crystalline graphitic structure of the carbon cores of the C-dots, displaying the in-plane lattice spacing of 0.215 nm corresponding to the [110] plane of graphite.[21] X-ray photoelectron spectroscopy (XPS) analysis further confirmed the structural integrity of the TTA–C-dots (Figure S3).

We further examined the effect of C-dot formation on the properties of the aerogel matrix, particularly its overall porosity, a critical parameter in the context of sensing applicability. Specifically, Brunauer–Emmett–Teller (BET) analysis of the TTA–C-dot–aerogel, shown in Figure 2C, indicates a relatively high specific surface area of 450 m^2/g (Figure 2C,i), average pore diameter of 4.8 nm (Figure 2C,ii), and pore volume of 0.51 cm^3/g. These values are similar to those of pristine aerogels (not containing embedded C-dots), confirming that the open porous structure of the aerogel was retained after the in situ synthesis process.

Fluorescence Sensing of Lanthanide and Actinide Metal Ions. Application of the TTA–C-dot–aerogel hybrid for the detection of lanthanide and actinide ions is depicted in Figures 3 and 4. Figure 3A presents the fluorescence emission spectra recorded following the addition of aqueous solutions of UO_2^{2+}, Eu^{3+}, or Sm^{3+} ions to the TTA–C-dot/aerogel. The fluorescence spectra in Figure 3A reveal two distinct effects. Specifically, a significant red shift of the emission peak, from 445 to 480 nm (excitation at 400 nm), occurred upon addition of UO_2^{2+} to the TTA–C-dot–aerogel (Figure 3A). Importantly, to the best of our knowledge, this is the first report on ion-induced red shift of C-dot fluorescence. This shift is likely

DOI: 10.1021/acsomega.7b01883
ACS Omega 2017, 2, 9288–9295

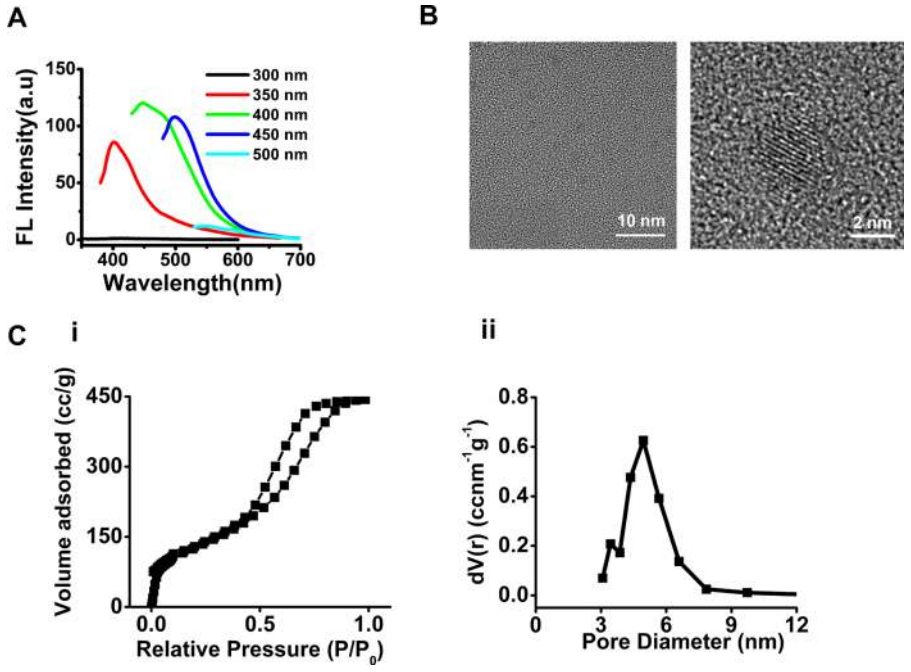

Figure 2. Characterization of the TTA−carbon-dot−aerogel. (A) Excitation-dependent emission spectra of the C-dots in C-dot−aerogel. (B) High-resolution transmission electron microscopy (HRTEM) images of C-dots extracted from the aerogel. The crystal planes of the C-dot graphitic core are apparent. (C) Brunauer−Emmett−Teller (BET) analysis of the TTA−C-dot−aerogel. (i) N_2 adsorption−desorption isotherms. (ii) Pore size distribution curve indicating an average pore size of 4.8 nm.

due to changes in electron density at the C-dots' surface because of coordination of the UO_2^{2+}/TTA chelating complex.[43] Red fluorescence shifts in case of conjugated polymers which form chelate with metal ions have been reported and ascribed to the modulation of conjugation network and surface electron densities.[43] The other effect highlighted in Figure 3A is fluorescence quenching induced upon addition of Eu^{3+} and Sm^{3+} ions to the TTA−C-dot/aerogel; the quenching effect was particularly apparent upon excitation at 350 nm (Figure 3A, right panel).

To investigate whether the significant ion-induced fluorescence modulation of the C-dot−aerogel in Figure 3A (shifts of emission peaks or fluorescence quenching) was due to the use of TTA as the carbonaceous precursor, we further tested a C-dot−aerogel hybrid in which the embedded C-dots were synthesized in situ from a different precursor, 6-*O*-(*O*-*O*′-dilauroyl-tartaryl)-D-glucose (Figure 3B). Indeed, Figure 3B demonstrates that neither emission shifts nor fluorescence quenching was induced upon the addition of UO_2^{2+}, Eu^{3+}, or Sm^{3+} ions to the C-dot−aerogel not prepared from TTA as the carbon source. These results are significant, as they clearly underscore the central role of the TTA units in determining the sensing features of the new TTA−C-dot−aerogel hybrid. The TTA−C-dot−aerogel system can also be employed for sensing lanthanide ions through fluorescence microscopy (Figure 3C). The confocal fluorescence microscopy images in Figure 3C (exc. 405 nm) show that the initial bright fluorescence of the C-dot−aerogel particles was substantially quenched upon addition of Sm^{3+} ions. Notably, a direct relationship between Sm^{3+} concentration and the extent of fluorescence signal attenuation was clearly apparent (Figure S4).

Figure 4 highlights the sensitivity and selectivity features of the new TTA−C-dot−aerogel hybrid. Figure 4A depicts the concentration-dependent shifts of the fluorescence emission (excitation 400 nm) upon addition of UO_2^{2+}, Sm^{3+}, or Eu^{3+}. Notably, only UO_2^{2+} induced an experimentally significant fluorescence shift, recorded even in low (<10 ppm) concentrations (Figure 4A). The graph in Figure 4B, depicting the fluorescence quenching (excitation 350 nm, emission 405 nm) versus ion concentrations, confirms the direct relationship between metal ion concentrations and the extent of C-dots' fluorescence quenching, indicating that adsorption of the ions within the aerogel pores accounted for the fluorescence quenching effect. Importantly, Figure 4B also indicates that the most pronounced fluorescence quenching of the C-dots' fluorescence was induced by the Sm^{3+} ion, reflected in the detection threshold of 0.5 ppm. Lesser, albeit experimentally significant, fluorescence quenching was induced by UO_2^{2+} and Eu^{3+} ions at higher concentrations. Although metal-ion-induced quenching of C-dots' fluorescence has been widely reported,[5,6] Figure 4B provides an extraordinary demonstration of selective lanthanide-induced fluorescence quenching via specifically tailored C-dots.

The bar diagrams in Figure 4C,D highlight the selectivity of the TTA−C-dot−aerogel platform. Significantly lesser fluorescence shifts (Figure 4C) or quenching (Figure 4D) was recorded upon addition of ions such as Cd^{2+}, Pb^{2+}, and Na^+ to the TTA−C-dot−aerogel. The selectivity of the TTA−C-dot/aerogel hybrid for UO_2^{2+} (fluorescence shift) and Sm^{3+} and Eu^{3+} (fluorescence quenching) likely reflects the high affinity of TTA toward these ions.[44−46] The pronounced binding of the ions to the TTA units at the C-dot surface affects their surface energy states, likely accounting for metal-ion-induced quenching of C-dot fluorescence.[23] The TTA-C-dots synthesized inside the aerogel host was extracted and excitation dependent emission property was observed in Figure S5 which revealed the similar property like Figure 2A.

To further probe the effects of the lanthanide and actinide ions on the TTA−C-dots encapsulated within the aerogel

DOI: 10.1021/acsomega.7b01883
ACS Omega 2017, 2, 9288−9295

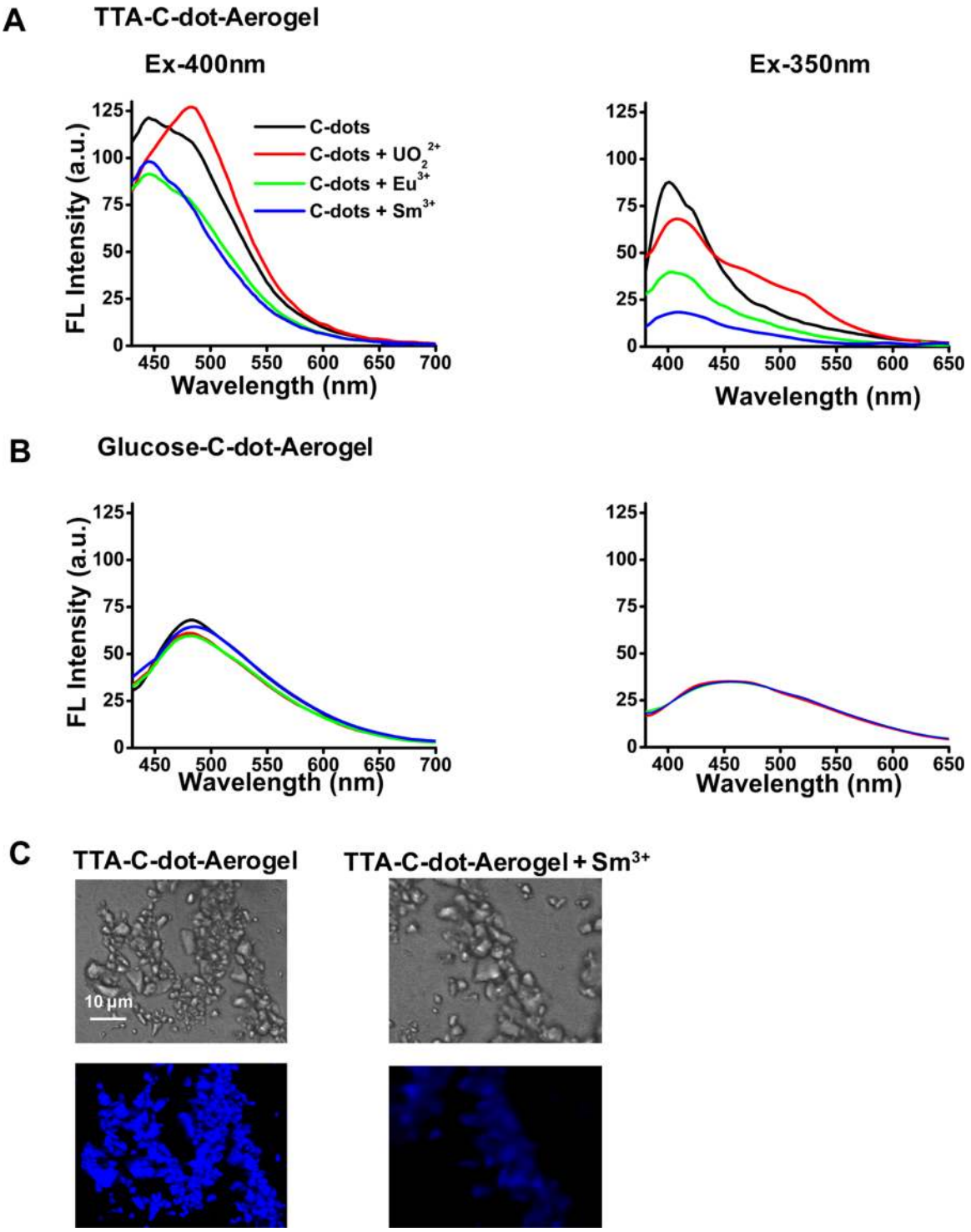

Figure 3. Effect of lanthanide and actinide ions on the fluorescence properties of C-dot−aerogels. (A, B) Fluorescence emission spectra (excitation wavelengths indicated) recorded following addition of the indicated ions: (A) TTA−C-dot−aerogel and (B) glucose derivative-C-dot−aerogel. (C) Confocal fluorescence microscopy images (exc. 405 nm and emission filter EM 445/60) of the TTA−C-dot−aerogel before and after the addition of Sm^{3+} ions (concentration 100 ppm).

matrix, we carried out Raman scattering experiments (Figure 5). The Raman spectra in Figure 5 corroborate the fluorescence data in Figures 3 and 4, indicating significant ion-dependent modifications of the TTA−C-dots surface units. The Raman spectrum of the untreated TTA−C-dot−aerogel (Figure 5i) exhibits several vibrations ascribed to the TTA unit,[47] including two main peaks around 1418 cm^{-1} assigned to the symmetric C═C−C═C stretching of the thienyl group and a vibration band at 1522 cm^{-1} assigned to the C═C−C═O stretching.

The effects of Sm^{3+} (Figure 5ii) and UO_2^{2+} (Figure 5iii) on the Raman spectra were significant and attributed to metal-induced conformational changes of the residual TTA on the C-dots' surface. Specifically, the main peak at 1417 cm^{-1} splits

DOI: 10.1021/acsomega.7b01883
ACS Omega 2017, 2, 9288−9295

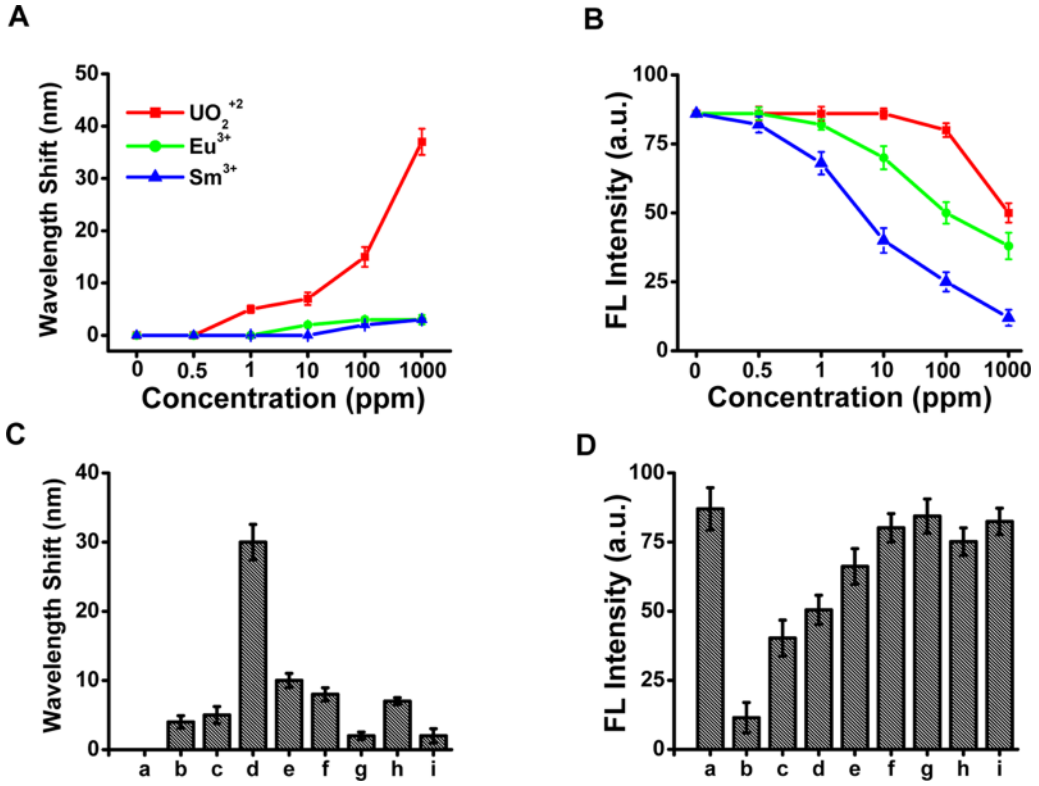

Figure 4. Fluorescence modulation of the TTA−C-dot−aerogel upon addition of metal ions. Concentration-dependent (A) shifts of the fluorescence peak (λ_{ex} 400 nm/λ_{em} 445 nm) and (B) intensity (λ_{ex} 350 nm/λ_{em} 405 nm). Comparison of the (C) fluorescence shifts (λ_{ex} 400 nm/λ_{em} 445 nm) and (D) fluorescence intensities (λ_{ex} 350 nm/λ_{em} 405 nm) upon addition of different metal ions: (a) control TTA−C-dot/aerogel, (b) Sm^{3+}, (c) Eu^{3+}, (d) UO_2^{2+}, (e) Ce^{3+}, (f) Nd^{3+}, (g) Gd^{3+}, (h) Cd^{2+}, and (i) Pb^{2+}. All ions were at a concentration of 100 ppm.

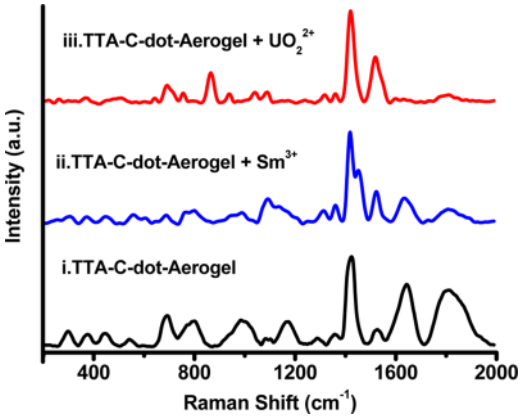

Figure 5. Raman spectra of the TTA−C-dots−aerogel. Ion concentrations were 100 ppm.

upon addition of Sm^{3+}, giving rise to a shoulder at 1447 cm^{-1}. Likewise, the Raman signal at 1526 cm^{-1} is more intense following the addition of either UO_2^{2+} or Sm^{3+} ions compared to that with the bare TTA−C-dot. Notably, the peak at 1610 cm^{-1}, corresponding to the C═C−C═O unit coupled to the OH bending mode (enolate form),[48] disappeared upon incubation of the TTA−C-dot−aerogel with UO_2^{2+} (Figure 5iii). This spectral modification is ascribed to the interaction between the OH group and the uranyl ion. Furthermore, the weaker vibrational bands at 400−790 cm^{-1} in the presence of the two ions may be traced to covalent interactions between the TTA−C-dot and the metal ions.[49,50] Overall, the Raman scattering data provide structural evidence for both retention of the TTA units on the C-dots and participation of the TTA residues in the interactions with UO_2^{2+}, Sm^{3+}, and Eu^{3+}. These interactions likely account for the significant fluorescence shifts and changes in intensities induced by the ions.

CONCLUSIONS

We present a new fluorescent sensor for lanthanide and actinide metal ions based on TTA-generated C-dots prepared in situ within the porous framework of silica aerogel. The structural and physical properties of both the aerogel matrix and embedded C-dots were retained following the synthesis procedure. Importantly, the aerogel framework was critical for the assembly of the fluorescent C-dots. The TTA−C-dot−aerogel hybrid constituted a selective and sensitive fluorescence sensor for UO_2^{2+}, Sm^{3+}, and Eu^{3+} ions, which gave rise to significant red shift of the C-dots' fluorescence (in case of UO_2^{2+}) or dramatic fluorescence quenching (Sm^{3+} and Eu^{3+}). The TTA−C-dot−aerogel sensor exhibits notable practical advantages. Preparation of the hybrid C-dot/aerogel material is straightforward, using inexpensive and readily available reagents. The TTA−C-dot−aerogel can be stored as a powder for long time periods. Sensing experiments are easy to perform and can be carried out through either fluorescence spectroscopy or microscopy. Importantly, the selectivity and sensitivity of the C-dot−aerogel sensor are on par or better than those of most lanthanide/actinide sensors reported thus far. This work further underscores the versatility of C-dots/aerogel constructs as sensing platforms for diverse analytes.

DOI: 10.1021/acsomega.7b01883
ACS Omega 2017, 2, 9288−9295

EXPERIMENTAL SECTION

Materials. Tetraethylorthosilicate (TEOS), 2-thenoyltrifluoroacetone (TTA), D-(+)-glucose, sodium sulfate, pyridine, ammonium hydroxide, lead nitrate, and cadmium nitrate were purchased from Sigma-Aldrich. L-(+)-Tartaric acid and sodium hydroxide were purchased from Alfa-Aesar, England. Lauroyl chloride was purchased from TCI, Japan. Europium chloride hexahydrate and samarium chloride hexahydrate were purchased from Strem Chemicals Inc. Uranyl nitrate hexahydrate ($UO_2(NO_3)_2{\cdot}6H_2O$) was purchased from Inorganic Ventures, Inc. Ethanol was purchased from J. T. Baker. Diethyl ether, ethyl acetate, and concentrated hydrochloric acid (HCl) were purchased from Bio Lab Ltd, Jerusalem, Israel.

Aerogel Synthesis. Wet silica gel was prepared according to previous reports.[17,33] Briefly, 5 mL of TEOS, 15 mL of anhydrous ethanol (EtOH), 5 mL of distilled water, and 5 μL of concentrated hydrochloric acid were mixed in a 100 mL flask and stirred in a 60 °C water bath for 90 min. Subsequently, 25 mL of ethanol, 13 mL of distilled water, and 15 μL of NH_4OH were added to the solution and stirred for 30 min at the same temperature. The prepared wet silica gel was coated with parafilm before it was further dried and transferred into 200 mL of anhydrous ethanol and placed in a GCF1400 atmosphere furnace under an ultrapure N_2 gas atmosphere. The outlet was subsequently closed while the ultrapure N_2 was continuously passed into the autoclave and it reached 1 MPa. The temperature was first raised quickly from room temperature to 200 °C, increased slowly to 246 °C, followed by 260 °C for 3 h at 2 MPa N_2 gas pressure. White silica aerogel was obtained after opening the autoclave.

In Situ Synthesis of TTA−C-Dot−Aerogel. Around 50 mg of the TTA precursor was mixed with 200 mg of aerogel in a glass vial, and 300 μL of diethyl ether and 500 μL of distilled water were added to the mixture. The suspension was then sonicated for 5 min and heated at 140 °C for 6 h. The synthesized C-dot−aerogel was purified by diethyl ether several times to remove C-dots that were not embedded within the aerogel.

TTA−C-Dot Synthesis in Aqueous Solution (without Aerogel). Around 50 mg of the TTA precursor was dissolved in 300 μL of diethyl ether, and 500 μL of distilled water was added to the mixture. The suspension was then sonicated for 5 min and heated at 140 °C for 6 h.

In Situ Synthesis of Glucose Derivative-C-Dot−Aerogel. Carbon dot precursor 6-*O*-(*O*-*O*′-dilauroyl-tartaryl)-D-glucose was synthesized according to our published report.[17] Around 10 mg of the C-dot precursor was mixed with 100 mg of aerogel in a glass vial, and 300 μL of distilled water was added to the mixture. The suspension was then sonicated and heated at 125 °C for 2.5 h. The synthesized C-dots−aerogel was purified by $CHCl_3$ several times to remove the unbound C-dots.

Ion Sensing. Metal ions were dissolved in distilled water at different concentrations (1−1000 ppm). Then, 50 μL of each ion was placed upon 50 mg of the C-dot−aerogel powder and incubated for 10 min. Fluorescence of the C-dot−aerogel slurry was recorded with different excitation wavelengths.

Instrumentation and Characterization. High-resolution transmission electron microscopy (HRTEM) experiments were carried out using TTA−C-dot−aerogel dissolved in chloroform for extraction of the carbon dots from the aerogel matrix. The HRTEM samples were prepared by placing a drop of solution on a graphene-coated copper grid and observed with a 200 kV JEOL JEM-2100F microscope (Japan). Fluorescence emission spectra of the C-dot−aerogel using different excitation wavelengths were recorded on a Varioskan plate reader. Confocal microscopy images were acquired on an Ultra View system (PerkinElmer Life Sciences, Waltham, MA) equipped with an Axiovert-200 M microscope (Zeiss, Oberkochen, Germany) and a Plan-Neofluar 63×/1.4 oil objective with 405 nm laser excitation wavelength. Raman spectra were recorded with a Horiba-Jobin-Yvon LabRam HR 800 micro-Raman system, equipped with a Synapse CCD detector. The excitation source was an argon laser (514.5 nm), with a power of 5 mW. The laser was focused with a 100× long-focal-length objective to a spot of about 1 μm. Measurements were taken with 600 g/mm grating and a confocal hole of 100 μm with a typical exposure time of 1 min.

ASSOCIATED CONTENT

Supporting Information

The Supporting Information is available free of charge on the ACS Publications website at DOI: 10.1021/acsomega.7b01883.

Excitation−emission spectra of TTA−C-dots in solution (Figure S1), size distribution histogram of TTA−C-dots in aerogel (Figure S2), XPS spectra of TTA−C-dots−aerogel (Figure S3), confocal image of TTA−C-dots−aerogel after Sm^{3+} sensing with different concentrations (Figure S4), and excitation-emission spectra of extracted TTA-C-dots from aerogel host (Figure S5) (PDF)

AUTHOR INFORMATION

Corresponding Authors

*E-mail: ofrapt@nrcn.org.il (O.P.-T.).
*E-mail: razj@bgu.ac.il (R.J.).

ORCID

Raz Jelinek: 0000-0002-0336-1384

Present Address

‖Schulich Faculty of Chemistry, Technion-Israel Institute of Technology, Haifa 3200003, Israel (S.K.B.)

Author Contributions

The manuscript was written through contributions of all authors. All authors have given approval to the final version of the manuscript.

Funding

This research was supported by the Pazi Foundation, grant number 285-17.

Notes

The authors declare no competing financial interest.

ACKNOWLEDGMENTS

Dr. Susanta Kumar Bhunia is grateful to the Planning and Budgeting Committee (PBC) of the Israeli Council for Higher Education for an Outstanding Post-Doctoral Fellowship.

REFERENCES

(1) Eisenbud, M.; Gesell, T. F. *Environmental Radioactivity from Natural, Industrial and Military Sources: From Natural, Industrial and Military Sources*, 4th ed.; Academic Press: San Diego, 1997; pp 1−656.
(2) Kumar, A.; Ali, M.; Ningthoujam, R. S.; Gaikwad, P.; Kumar, M.; Nath, B. B.; Pandey, B. N. The interaction of actinide and lanthanide

DOI: 10.1021/acsomega.7b01883
ACS Omega 2017, 2, 9288−9295

ions with hemoglobin and its relevance to human and environmental toxicology. *J. Hazard. Mater.* **2016**, *307*, 281−293.
(3) Pandey, B. N.; Kumar, A.; Tiwari, P.; Mishra, K. P. Radiobiological basis in management of accidental radiation exposure. *Int. J. Radiat. Biol.* **2010**, *86*, 613−635.
(4) Blais, J.; Djedidi, Z.; Cheikh, R. B.; Tyagi, R.; Mercier, G. Metals precipitation from effluents. *Pract. Period. Hazard., Toxic, Radioact. Waste Manage.* **2008**, *12*, 135−149.
(5) Wang, Z.; Xu, C.; Lu, Y.; Chen, X.; Yuan, H.; Wei, G.; Ye, G.; Chen, J. Fluorescence sensor array based on amino acid derived carbon dots for pattern-based detection of toxic metal ions. *Sens. Actuators, B* **2017**, *241*, 1324−1330.
(6) Wang, Z.; Xu, C.; Lu, Y.; Wu, F.; Ye, G.; Wei, G.; Sun, T.; Chen, J. Visualization of Adsorption: Luminescent Mesoporous Silica-Carbon Dots Composite for Rapid and Selective Removal of U (VI) and in Situ Monitoring the Adsorption Behavior. *ACS Appl. Mater. Interfaces* **2017**, *9*, 7392−7398.
(7) Ganjali, M. R.; Ravanshad, J.; Hosseini, M.; Salavati-Niasari, M.; Pourjavid, M. R.; Baezzat, M. R. Novel Dy (III) sensor based on a new bis-pyrrolidene Schiff's base. *Electroanalysis* **2004**, *16*, 1771−1776.
(8) Lisowski, C. E.; Hutchison, J. E. Malonamide-functionalized gold nanoparticles for selective, colorimetric sensing of trivalent lanthanide ions. *Anal. Chem.* **2009**, *81*, 10246−10253.
(9) Bekiari, V.; Judeinstein, P.; Lianos, P. A sensitive fluorescent sensor of lanthanide ions. *J. Lumin.* **2003**, *104*, 13−15.
(10) Das, P.; Ghosh, A.; Das, A. Unusual specificity of a receptor for Nd3+ among other lanthanide ions for selective colorimetric recognition. *Inorg. Chem.* **2010**, *49*, 6909−6916.
(11) Ritchie, J.; Ruseckas, A.; André, P.; Münther, C.; Van Ryssen, M.; Vize, D. E.; Crayston, J. A.; Samuel, I. D. Synthesis and lanthanide-sensing behaviour of polyfluorene/1, 10-phenanthroline copolymers. *Synth. Met.* **2009**, *159*, 583−588.
(12) Wang, S.; Ding, L.; Fan, J.; Wang, Z.; Fang, Y. Bispyrene/surfactant-assembly-based fluorescent sensor array for discriminating lanthanide ions in aqueous solution. *ACS Appl. Mater. Interfaces* **2014**, *6*, 16156−16165.
(13) Gole, B.; Bar, A. K.; Mukherjee, P. S. Fluorescent metal-organic framework for selective sensing of nitroaromatic explosives. *Chem. Commun.* **2011**, *47*, 12137−12139.
(14) Zhang, J. F.; Lim, C. S.; Bhuniya, S.; Cho, B. R.; Kim, J. S. A highly selective colorimetric and ratiometric two-photon fluorescent probe for fluoride ion detection. *Org. Lett.* **2011**, *13*, 1190−1193.
(15) Kim, H. N.; Ren, W. X.; Kim, J. S.; Yoon, J. Fluorescent and colorimetric sensors for detection of lead, cadmium, and mercury ions. *Chem. Soc. Rev.* **2012**, *41*, 3210−3244.
(16) Clark, D. L.; Hobart, D. E.; Neu, M. P. Actinide carbonate complexes and their importance in actinide environmental chemistry. *Chem. Rev.* **1995**, *95*, 25−48.
(17) Dolai, S.; Bhunia, S. K.; Jelinek, R. Carbon-dot-aerogel sensor for aromatic volatile organic compounds. *Sens. Actuators, B* **2017**, *241*, 607−613.
(18) Ali, H.; Bhunia, S. K.; Dalal, C.; Jana, N. R. Red fluorescent carbon nanoparticle-based cell imaging probe. *ACS Appl. Mater. Interfaces* **2016**, *8*, 9305−9313.
(19) Bhunia, S. K.; Nandi, S.; Shikler, R.; Jelinek, R. Tuneable light-emitting carbon-dot/polymer flexible films prepared through one-pot synthesis. *Nanoscale* **2016**, *8*, 3400−3406.
(20) Bhunia, S. K.; Saha, A.; Maity, A. R.; Ray, S. C.; Jana, N. R. Carbon nanoparticle-based fluorescent bioimaging probes. *Sci. Rep.* **2013**, *3*, No. 1473.
(21) Bhunia, S. K.; Maity, A. R.; Nandi, S.; Stepensky, D.; Jelinek, R. Imaging cancer cells expressing the folate receptor with carbon dots produced from folic acid. *ChemBioChem* **2016**, *17*, 614−619.
(22) Baker, S. N.; Baker, G. A. Luminescent carbon nanodots: emergent nanolights. *Angew. Chem., Int. Ed.* **2010**, *49*, 6726−6744.
(23) Gao, X.; Du, C.; Zhuang, Z.; Chen, W. Carbon quantum dot-based nanoprobes for metal ion detection. *J. Mater. Chem. C* **2016**, *4*, 6927−6945.
(24) Zhang, J.; Yu, S.-H. Carbon dots: large-scale synthesis, sensing and bioimaging. *Mater. Today* **2016**, *19*, 382−393.
(25) Dhenadhayalan, N.; Lin, K.-C. Chemically induced fluorescence switching of carbon-dots and its multiple logic gate implementation. *Sci. Rep.* **2015**, *5*, No. 10012.
(26) Zhang, Z.; Shi, Y.; Pan, Y.; Cheng, X.; Zhang, L.; Chen, J.; Li, M.-J.; Yi, C. Quinoline derivative-functionalized carbon dots as a fluorescent nanosensor for sensing and intracellular imaging of Zn2+. *J. Mater. Chem. B* **2014**, *2*, 5020−5027.
(27) Cui, X.; Zhu, L.; Wu, J.; Hou, Y.; Wang, P.; Wang, Z.; Yang, M. A fluorescent biosensor based on carbon dots-labeled oligodeoxyribonucleotide and graphene oxide for mercury (II) detection. *Biosens. Bioelectron.* **2015**, *63*, 506−512.
(28) Moore, F. L. In *Metals Analysis with Thenoyltrifluoroacetone*, Symposium on Solvent Extraction in the Analysis of Metals; ASTM International: 1958.
(29) Vigato, P. A.; Peruzzo, V.; Tamburini, S. The evolution of β-diketone or β-diketophenol ligands and related complexes. *Coord. Chem. Rev.* **2009**, *253*, 1099−1201.
(30) Roundhill, D. M. Extraction of Actinides and Lanthanides. In *Extraction of Metals from Soils and Waters*; Springer, 2001; pp 193−230.
(31) Poskanzer, A.; Foreman, B. A summary of TTA extraction coefficients. *J. Inorg. Nucl. Chem.* **1961**, *16*, 323−336.
(32) Abubacker, K.; Prasad, N. K. Studies on TTA complexes with metal ions-I: spectrophotometric and potentiometric investigations on uranyl complexes. *J. Inorg. Nucl. Chem.* **1961**, *16*, 296−307.
(33) Dolai, S.; Bhunia, S. K.; Beglaryan, S. S.; Kolusheva, S.; Zeiri, L.; Jelinek, R. Colorimetric Polydiacetylene-Aerogel Detector for Volatile Organic Compounds (VOCs). *ACS Appl. Mater. Interfaces* **2017**, *9*, 2891−2898.
(34) Li, L.; Yalcin, B.; Nguyen, B. N.; Meador, M. A. B.; Cakmak, M. Flexible nanofiber-reinforced aerogel (xerogel) synthesis, manufacture, and characterization. *ACS Appl. Mater. Interfaces* **2009**, *1*, 2491−2501.
(35) Zou, J.; Liu, J.; Karakoti, A. S.; Kumar, A.; Joung, D.; Li, Q.; Khondaker, S. I.; Seal, S.; Zhai, L. Ultralight multiwalled carbon nanotube aerogel. *ACS Nano* **2010**, *4*, 7293−7302.
(36) Kristiansen, T.; Mathisen, K.; Einarsrud, M.-A.; Bjørgen, M.; Nicholson, D. G. Single-site copper by incorporation in ambient pressure dried silica aerogel and xerogel systems: an X-ray absorption spectroscopy study. *J. Phys. Chem. C* **2011**, *115*, 19260−19268.
(37) Chervin, C. N.; Clapsaddle, B. J.; Chiu, H. W.; Gash, A. E.; Satcher, J. H.; Kauzlarich, S. M. Aerogel Synthesis of Yttria-Stabilized Zirconia by a Non-Alkoxide Sol-Gel Route. *Chem. Mater.* **2005**, *17*, 3345−3351.
(38) Boday, D. J.; Stover, R. J.; Muriithi, B.; Keller, M. W.; Wertz, J. T.; DeFriend Obrey, K. A.; Loy, D. A. Strong, low-density nanocomposites by chemical vapor deposition and polymerization of cyanoacrylates on aminated silica aerogels. *ACS Appl. Mater. Interfaces* **2009**, *1*, 1364−1369.
(39) Randall, J. P.; Meador, M. A. B.; Jana, S. C. Tailoring mechanical properties of aerogels for aerospace applications. *ACS Appl. Mater. Interfaces* **2011**, *3*, 613−626.
(40) Wang, D.; McLaughlin, E.; Pfeffer, R.; Lin, Y. Adsorption of organic compounds in vapor, liquid, and aqueous solution phases on hydrophobic aerogels. *Ind. Eng. Chem. Res.* **2011**, *50*, 12177−12185.
(41) Wang, R.; Li, G.; Dong, Y.; Chi, Y.; Chen, G. Carbon quantum dot-functionalized aerogels for NO2 gas sensing. *Anal. Chem.* **2013**, *85*, 8065−8069.
(42) Bheekhun, N.; Talib, A. R. A.; Hassan, M. R. Aerogels in aerospace: an overview. *Adv. Mater. Sci. Eng.* **2013**, *2013*, 1−18.
(43) Wang, B.; Wasielewski, M. R. Design and synthesis of metal ion-recognition-induced conjugated polymers: an approach to metal ion sensory materials. *J. Am. Chem. Soc.* **1997**, *119*, 12−21.
(44) Zhang, G.-C.; Li, D.-D.; Kong, M.; Su, J.; Zhou, H.-P.; Wu, J.-Y.; Tian, Y.-P. Synthesis, Crystal Structures, and Photophysical Properties Investigations of Two New Pyridinium Complexes

DOI: 10.1021/acsomega.7b01883
ACS Omega 2017, 2, 9288−9295

Containing [Sm(TTA)4]- and [Eu (TTA)4]-. *Synth. React. Inorg., Met.-Org., Nano-Met. Chem.* **2016**, *46*, 1254−1259.
(45) Barrett, C. A.; Chouyyok, W.; Speakman, R. J.; Olsen, K. B.; Addleman, R. S. Rapid extraction and assay of uranium from environmental surface samples. *Talanta* **2017**, *173*, 69−78.
(46) Kamata, E.; Nakashima, R.; Furukawa, M. Determination of trace amounts of thorium and uranium in coal ash by inductively coupled plasma atomic emission spectrometry after extraction with 2-thenoyltrifluoroacetone and back-extraction with dilute nitric acid. *J. Anal. At. Spectrom.* **1987**, *2*, 321−324.
(47) Nekoei, A.-R.; Tayyari, S. F.; Vakili, M.; Holakoei, S.; Hamidian, A. H.; Sammelson, R. E. Conformation and vibrational spectra and assignment of 2-thenoyltrifluoroacetone. *J. Mol. Struct.* **2009**, *932*, 112−122.
(48) Sun, Q.; Zheng, H. Raman OH stretching vibration of ice I h. *Prog. Nat. Sci.* **2009**, *19*, 1651−1654.
(49) Elving, P. J.; Callahan, C. M. Polarographic Behavior of Thenoyltrifluoroacetone (TTA) and Related Compounds. Alkaline Cleavage of TTA. Complexation of TTA with Borate. Analytical Determination of TTA. *J. Am. Chem. Soc.* **1955**, *77*, 2077−2082.
(50) Edwards, H.; Hughes, M.; Smith, D. Raman microscopic studies of the liquid-liquid interface between an organic layer and an aqueous solution containing metal ions. *Vib. Spectrosc.* **1996**, *10*, 281−289.

DOI: 10.1021/acsomega.7b01883
ACS Omega 2017, 2, 9288−9295